*Clays and Clay Minerals*, Vol. 48, No. 4, 446–458, 2000.

# EVOLUTION OF FUNDAMENTAL-PARTICLE SIZE DURING ILLITIZATION OF SMECTITE AND IMPLICATIONS FOR REACTION MECHANISM

J. ŚRODOŃ,[1] D.D. EBERL,[2] AND V.A. DRITS[3]

[1] Institute of Geological Sciences PAN, Senacka 1, 31002 Kraków, Poland
[2] U.S. Geological Survey, 3215 Marine St., Boulder, Colorado 80303-1066, USA
[3] Institute of Geology RAN, Pyzhevsky 7, 109017 Moscow, Russia

**Abstract**—Area-weighted thickness distributions of fundamental illite particles for samples of illite and illite-smectite from seven locations (including bentonites and hydrothermally altered pyroclastics) were measured by Pt-shadowing technique, by transmission electron microscopy. Most thickness distributions are described by lognormal distributions, which suggest a unique crystallization process. The shapes of lognormal distributions of fundamental illite particles can be calculated from the distribution mean because the shape parameters $\alpha$ and $\beta^2$ are interrelated: $\beta^2 = 0.107\alpha - 0.03$. This growth process was simulated by the mathematical Law of Proportionate Effect that generates lognormal distributions. Simulations indicated that illite particles grow from 2-nm thick illite nuclei by surface-controlled growth, *i.e.*, the rate of growth is restricted by how rapid crystallization proceeds given a near infinite supply of reactants, and not by the rate of supply of reactants to the crystal surface. Initially formed, 2-nm thick crystals may nucleate and grow within smectite interlayers from material produced by dissolution of single smectite 2:1 layers, thereby transforming the clay from randomly interstratified (Reichweite, R = 0) to ordered (R = 1) illite-smectite after the smectite single layers dissolve. In this initial period of illite nucleation and growth, during which expandable layers range from 100 to 20%, illite crystals grow parallel to [001]* direction, and the dimensions of the (001) plane are confined to the size of the original smectite 2:1 layers. After nucleation ceases, illite crystals may continue to grow by surface-controlled growth, and the expandable-layer content ranges from 20 to 0%. This latter period of illitization is characterized by three-dimensional growth. Other crystal-growth mechanisms, such as Ostwald ripening, supply-controlled growth, and the coalescence of smectite layers, do not produce the observed evolution of $\alpha$ and $\beta^2$ and the observed shapes of crystal thickness distributions.

**Key Words**—Crystal Growth, Fundamental Particle, Illite-Smectite, Illitization Mechanism, Lognormal Distribution, Ostwald Ripening.

## INTRODUCTION

The term "fundamental particle" was introduced by Nadeau *et al.* (1984) to indicate the thinnest physically separable clay particles (*e.g.*, ~1 nm thickness for smectite particles, and 2 nm or larger thicknesses for illite particles) that produce single, hexagonal-based, electron diffraction patterns when observed in the transmission electron microscope (TEM). These authors used the Pt-shadowing technique to measure fundamental-particle thickness. We adopt this term, but with a different genetic connotation than that presented by Nadeau *et al.* (1984). In subsequent studies that used high-resolution (HR) TEM imaging of bulk-rock specimens processed to preserve the original fabric (Środoń *et al.*, 1990) and X-ray diffraction (XRD) analyses of bulk-rock specimens (Reynolds, 1992), most fundamental particles were found to occur as "building blocks" of mixed-layer crystals (MacEwan crystallites). The occurrence of fundamental illite particles as individual entities on TEM grids results from infinite osmotic swelling of mixed-layer crystals along the interlayers containing hydrated cations (*i.e.*, "smectitic interlayers"). Such swelling produces single 2:1 layers (smectite fundamental particles) and sets of 2:1 layers bonded by fixed and non-hydrated cations (illite fundamental particles). Infinite swelling of mixed-layer crystals can be achieved under the conditions involved in the preparation of electron microscope specimens (the use of Na or Li exchange cations and very dilute, electrolyte-free suspension). Illites are commonly thick particles where interparticle diffraction effects are minimal. Thus, the illite fundamental-particle thickness is identical to crystal thickness. Illite-smectites are minerals composed of thin illite particles with or without accompanying smectite single layers. The fundamental-particle size in illite-smectite is necessarily smaller than the mixed-layer crystal size of illite-smectite. With increasing percent of swelling interlayers, the number of fundamental particles per mixed-layer crystal gradually increases to about five for pure smectite (Drits *et al.*, 1997).

Nadeau *et al.* (1984) measured thickness distributions of fundamental particles from illite-smectites. Nadeau (1985, 1987) established several relations between fundamental-particle dimensions, including a positive correlation among the mean particle thickness, the mean area of the (001) plane, and the standard deviation of the thickness distribution. Inoue *et al.* (1987), Lanson and Champion (1991), and Inoue and

Kitagawa (1994) confirmed these findings, and showed that platelet shapes evolve during illitization: from irregular plates, to laths, to hexagons. Eberl and Środoń (1988) and Inoue *et al.* (1988) published additional sets of fundamental-particle size distributions, and interpreted them (probably incorrectly) as products of Ostwald ripening, *i.e.,* closed-system growth guided by surface free energy (large particles growing at the expense of dissolving small particles). Eberl *et al.* (1990) recognized that illitic samples do not follow the crystal-size distribution (CSD) shapes expected theoretically for Ostwald ripening according to the Lifshitz-Slyozov-Wagner theory (Eberl *et al.,* 1998a), but they do follow a lognormal distribution. The present contribution analyzes in detail the CSD of illite fundamental particles, and interprets the illitization mechanism from these data, using the model (Eberl *et al.,* 1998a) of the evolution of CSD in open and closed systems.

## CHARACTERISTICS OF THE LOGNORMAL DISTRIBUTION

A random variable X follows the lognormal distribution if the logarithms of X, ln(X), obey the normal probability distribution. A probability density function, g(X), which describes the theoretical lognormal frequency distribution of X, is given by:

$$g(X) = \left[\frac{1}{X\beta\sqrt{2\pi}}\right]\exp\left\{-\left(\frac{1}{2\beta^2}\right)[\ln(X) - \alpha]^2\right\}. \quad (1)$$

The parameters $\alpha$ and $\beta^2$ are the mean and the variance of ln(X), respectively, and they completely describe the distribution of X values. These parameters are determined by the following equations:

$$\alpha = \int \ln(X)f(X); \quad (2)$$

$$\beta^2 = \int [\ln(X) - \alpha]^2 f(X) \quad (3)$$

for the continuous frequency distribution f(X). In practice, we usually deal with discrete phenomena and observations ($X_i$ is an i-th measured value), and thus,

$$\alpha = \sum \ln(X_i)f(X_i); \quad (4)$$

$$\beta^2 = \sum [\ln(X_i) - \alpha]^2 f(X_i). \quad (5)$$

The lognormal distribution is skewed towards larger values, and the degree of skewness depends on the variance of ln(X). The lognormal distribution is characterized by moments, $\overline{X^n}$, *i.e.,* mean values of X raised to the power n:

$$\overline{X^n} = \sum X^n f(X) = \exp(n\alpha + n^2\beta^2/2). \quad (6)$$

First and second order moments, *i.e.,* mean values of X and $X^2$, are used in this study:

$$\overline{X} = \exp(\alpha + \beta^2/2) \quad (7)$$

$$\overline{X^2} = \exp(2\alpha + 2\beta^2). \quad (8)$$

## MATERIALS AND METHODS OF MEASUREMENT

TEM data used here were collected by several different analysts using the Pt-shadowing technique (Środoń *et al.,* 1992). The analyzed samples (Table 1) are pure fractions of illite and illite-smectite. These fractions were separated from altered pyroclastic rocks which have undergone burial diagenetic or hydrothermal alteration. Thus, all samples contain authigenic clays, free from detrital-illite contamination. All rocks were soft and swelled in water, and thus no grinding was needed prior to clay-fraction separation, thereby preserving natural crystal-thickness distributions. In hard rocks, grinding has been shown to cleave illite crystals (*e.g.,* Jiang *et al.,* 1997).

In our experience, distributions of fundamental particle thickness in the clay fraction of illite-smectite from diagenetically or hydrothermally altered pyroclastics is representative of the whole rock, provided that the clay is not separated into fractions of <0.2 μm and extreme dilutions are not used. With extreme dilutions, mixed-layer crystals undergo infinite osmotic swelling, and centrifugation may separate different populations of fundamental particles (Clauer *et al.,* 1997).

TEM measurement of the thickness of thin fundamental particles can be biased towards larger values owing to the tendency of the operator to select larger and "nice looking" particles if special precautions are not taken (Środoń *et al.,* 1992). All measurements analyzed in this study followed a standard procedure to avoid operator biases. Fundamental particles of illite are known to have variable dimensions in the (001) plane, which must be included in the crystal-size analysis. For this reason, HRTEM data, which consist exclusively of particle-thickness measurements, were not used in this study. Data sets (Table 1) consist of thickness, length, and width, and particle area, which is calculated as length times width.

## ANALYSIS OF PARTICLE-SIZE DATA

### *Particle-thickness distributions*

*Types of thickness distributions and measurement error.* Illite and smectite fundamental particles are plates with different shapes and dimensions in the (001) plane. Distributions of particle thicknesses can be analyzed as number-weighted (NW), (001) area-weighted (AW), or volume-weighted (VW) frequencies. Area-weighted distributions are most useful, because they relate to XRD and chemical measurements, including expandability by XRD on the basis of calculations from program NEWMOD (Reynolds, 1985),

Table 1. Selected XRD and TEM data for the studied samples.[1]

| Sample | No. particles | % smectite particles (TEM) | % S (XRD) | Ordering (XRD) | $\overline{N_a}$ (ID) | α (ID) | $\beta^2$ (ID) | $\overline{N_a}$ (ISD) | α (ISD) | $\beta^2$ (ISD) |
|---|---|---|---|---|---|---|---|---|---|---|
| *Upper Silesia (1)* | | | | | | | | | | |
| 2M9 | 114 | 76 | 88 | R = 0 | 2.00 | 0.69 | 0.00 | 1.24 | 0.17 | 0.09 |
| 3M2 | 68 | 57 | 45 | R = 0 | 2.15 | 0.75 | 0.03 | 1.50 | 0.33 | 0.15 |
| 1M6 | 128 | 6 | 41 | R = 1 | 2.32 | 0.82 | 0.04 | 2.24 | 0.77 | 0.07 |
| Ch5 | 266 | 7 | 39 | R = 1 | 2.46 | 0.87 | 0.05 | 2.35 | 0.81 | 0.10 |
| R62 | 112 | 2 | 29 | R = 1 | 2.65 | 0.94 | 0.07 | 2.62 | 0.92 | 0.09 |
| T9 | 149 | 3 | 20 | R > 1 | 2.76 | 0.98 | 0.07 | 2.72 | 0.95 | 0.10 |
| *Wales (2)* | | | | | | | | | | |
| M3 | 165 | 79 | 66 | R = 0 | 2.00 | 0.69 | 0.00 | 1.21 | 0.15 | 0.08 |
| M9 | 142 | 40 | 38 | R = 0 / R = 1 | 2.29 | 0.80 | 0.06 | 1.78 | 0.48 | 0.19 |
| M4 | 108 | 2 | 15 | R > 1 | 2.64 | 0.93 | 0.08 | 2.61 | 0.91 | 0.09 |
| M5 | 102 | 2 | 25 | R = 1 | 2.68 | 0.94 | 0.08 | 2.64 | 0.92 | 0.09 |
| M11 | 68 | 0 | 6 | R > 1 | 5.46 | 1.63 | 0.13 | | | |
| *San Juan Mts. (3)* | | | | | | | | | | |
| RM8 | 111 | 0 | 7 | R > 1 | 6.23 | 1.75 | 0.17 | | | |
| RM35A | 99 | 0 | 9 | R > 1 | 6.86 | 1.80 | 0.26 | | | |
| RM30 | 95 | 0 | 6 | R > 1 | 11.57 | 2.31 | 0.27 | | | |
| SG4 | 82 | 0 | 3 | R > 1 | 17.75 | 2.76 | 0.27 | | | |
| *Zempleni Hills (4)* | | | | | | | | | | |
| ZEMPLENI | 140 | 1 | 16 | R > 1 | 3.05 | 1.08 | 0.08 | 3.03 | 1.07 | 0.09 |
| *East Slovakia (5)* | | | | | | | | | | |
| CIC1/20 | 79 | 24 | 45 | R = 0 / R = 1 | 2.49 | 0.87 | 0.08 | 2.13 | 0.66 | 0.20 |
| CIC1/18 | 108 | 24 | 51 | R = 0 / R = 1 | 2.48 | 0.86 | 0.08 | 2.12 | 0.65 | 0.20 |
| CIC8/11 | 130 | 2 | 33 | R = 1 | 2.70 | 0.95 | 0.08 | 2.67 | 0.94 | 0.09 |
| TRH1/37 | 136 | 0 | 18 | R > 1 | 3.45 | 1.17 | 0.12 | | | |
| *Dolna Ves (6)* | | | | | | | | | | |
| DV4 | 119 | 2 | 45 | R = 1 | 2.21 | 0.78 | 0.03 | 2.18 | 0.76 | 0.05 |
| 2218 | 140 | 4 | 29 | R = 1 | 2.72 | 0.97 | 0.07 | 2.66 | 0.93 | 0.10 |
| 1555 | 142 | 0 | 21 | R > 1 | 2.89 | 1.02 | 0.08 | | | |
| 1603 | 141 | 0 | 8 | R > 1 | 4.38 | 1.42 | 0.12 | | | |
| *Kamikita (7)* | | | | | | | | | | |
| KAM-12-40 | 56 | 0 | 12 | R > 1 | 7.60 | 1.94 | 0.17 | | | |
| KAM-12-80 | 61 | 0 | 4 | R > 1 | 10.02 | 2.20 | 0.20 | | | |
| KAM-12-50 | 66 | 0 | 3 | R > 1 | 10.48 | 2.27 | 0.15 | | | |
| KAM-12-140 | 56 | 0 | 0 | illite | 12.49 | 2.46 | 0.13 | | | |
| KAM-12-262 | 43 | 0 | 0 | illite | 24.85 | 3.07 | 0.30 | | | |
| KAM-12-223 | 43 | 0 | 0 | illite | 28.21 | 3.22 | 0.25 | | | |
| KAM-12-290 | 58 | 0 | 0 | illite | 41.89 | 3.58 | 0.35 | | | |

[1] Number of fundamental particles measured by TEM, percent smectite particles in this population, XRD expandability, and ordering are presented along with the calculated parameters α, $\beta^2$, and mean thicknesses ($\overline{N_a}$) of area-weighted lognormal distributions of fundamental particles of illite (ID), and illite plus smectite (ISD). (1) Zoned Carboniferous bentonite from the Upper Silesia Coal Basin (Środoń *et al.*, 1986, 1992); (2) Silurian bentonites from Welsh Borderlands (*ibid.*); (3) Hydrothermally altered fault gauges from Silverton caldera, San Juan Mts., Colorado (Eberl *et al.*, 1987; Środoń *et al.*, 1992); (4) Hydrothermally altered rhyolite, Zempleni Hills, Hungary (Środoń *et al.*, 1992; Viczián, 1997); (5) Miocene bentonites from the East Slovak Basin (Šucha *et al.*, 1993); (6) Hydrothermally altered Miocene volcanics from central Slovakia (Šucha *et al.*, 1996); (7) Hydrothermally altered Miocene volcanics, Japan (Inoue and Kitagawa, 1994).

mean value of fundamental-particle thicknesses determined from fixed cations (Środoń *et al.*, 1992), and thickness distributions of mixed-layer crystals and fundamental particles as determined by the Bertaut-Warren-Averbach method (Drits *et al.*, 1998; Eberl *et al.*, 1998b).

An XRD technique for measuring mean thickness on the basis of integral peak width (Drits *et al.*, 1997) measures mean volume-weighted thickness (L, or "effective thickness"). L is related to the mean area-weighted thickness ($\overline{N_a}$):

$$L = \overline{N_a^2}/\overline{N_a} \quad (9)$$

where $\overline{N_a^2}$ is the mean of the squares of area-weighted thicknesses. For a lognormal distribution, Equations (7), (8), and (9) give the following relationship between the volume and the mean area-weighted thicknesses:

$$L = \overline{N_a}\exp(\beta^2). \quad (10)$$

Area-weighted frequency distributions were calculated by summation of areas (length × width) separately for each size class of fundamental particle thickness, and then by normalizing the sum of all areas to unity. These frequencies were used to calculate the

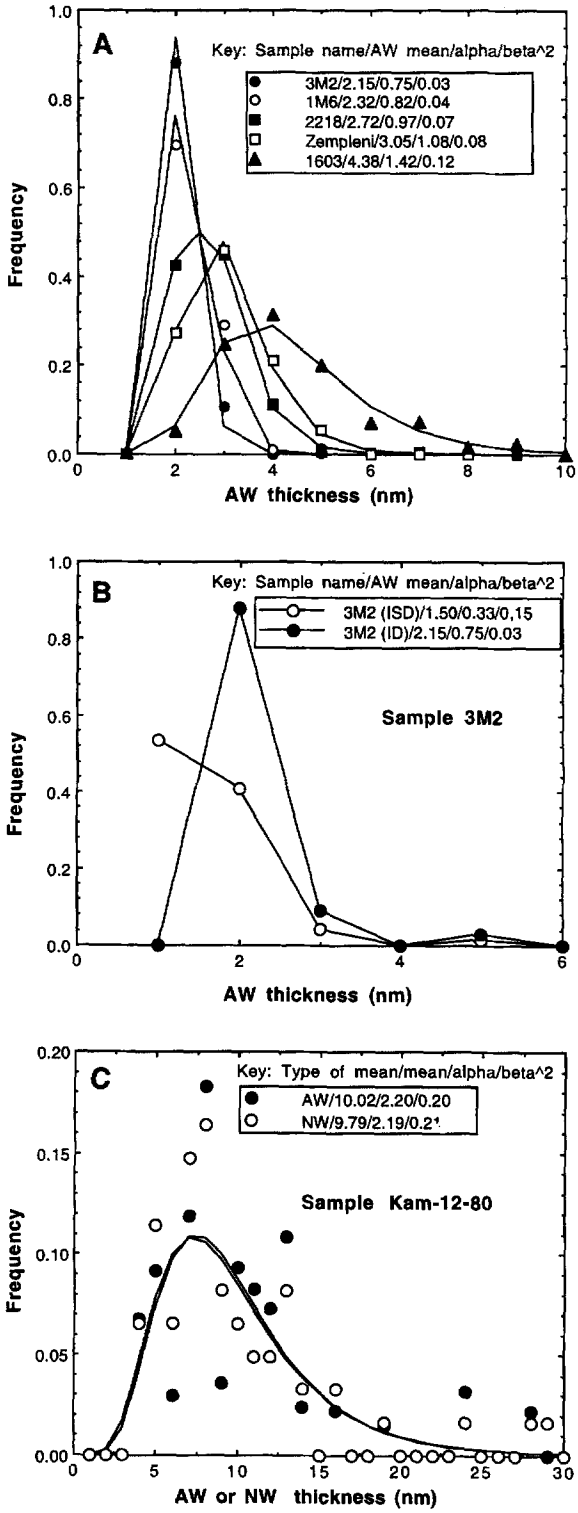


Figure 1. Examples of thickness distributions of fundamental particles from TEM measurements. Figure legends include sample name, the mean ($\overline{N}$ or $\overline{N_a}$), and the lognormal parameters alpha ($\alpha$) and beta$^2$ ($\beta^2$). The solid lines in Figures A and C are theoretical lognormal curves calculated for these parameters from Equation (1). A) area-weighted distributions of illite fundamental particles for five samples with different mean thicknesses; B) area-weighted thickness distributions of illite (ID) and illite + smectite (ISD) fundamental particles for the same randomly interstratified sample; C) area-weighted (AW) compared to particle number-weighted (NW) distributions of a sample with a large mean particle thickness. The scatter of data, owing to poor counting statistics, is larger for the AW distribution.

mean thickness ($\overline{N_a}$) and $\alpha$ and $\beta^2$ parameters [Equations (2) and (3)]. From these parameters, theoretical lognormal distributions were calculated [Equations (1), (4), and (5)] and compared with experimental data. Number-weighted frequencies were processed in an analogous manner. Mean thickness in this case is designated as $\overline{N}$, and this symbol also is used below if AW and NW distributions are considered jointly.

Illite-smectites of low expandability contain only one type of fundamental particle, *i.e.*, illite (Table 1), which is characterized by the presence of fixed interlayer cations. The chemical composition of such thin illite particles is affected strongly by the composition of their top and bottom surfaces, which may be different from their interior (Altaner *et al.*, 1988). Illite-smectite of higher expandability may contain such illite particles and smectite particles, *i.e.*, single 2:1 layers without fixed interlayer cations (Table 1). For samples containing both smectite particles and illite particles, two thickness distributions were calculated per sample: one for all fundamental particles (the illite + smectite distribution, or ISD) and one for illite particles only (ID). Table 1 lists the results of these calculations, and Figure 1 presents selected crystal-size distributions, covering a range of mean particle thicknesses. Calculated $\overline{N_a}$ or $\overline{N}$, and $\alpha$ and $\beta^2$ values are given in Figure 1, and theoretical lognormal distributions calculated from $\alpha$ and $\beta^2$ are plotted as solid lines in Figure 1A and 1C.

Area-weighted ID are smooth curves, and are in good agreement (except for clays with Reichweite, R = 0, see below) with theoretical lognormal curves if $\overline{N} < 6$ (Figure 1A). CSDs for these samples are lognormal at the >10% significance level, on the basis of the Kolmogorov-Smirnov statistical test (Benjamin and Cornell, 1970). The same is true for number-weighted distributions for $\overline{N} < 6$ (not shown). At higher $\overline{N}$, distributions become scattered, and the scatter is greater for the area-weighted distributions than for the number-weighted distributions (Figure 1C), especially at greater $\overline{N}$ values, which results from the fact that thicker particles have greater areas. The scatter results from poor counting statistics. At $\overline{N}$ = 3, 50 measurements are sufficient to obtain an estimate of $\alpha$ and $\beta^2$ to within a few percent. At larger $\overline{N}$ values, the distributions spread out, and there are more size classes

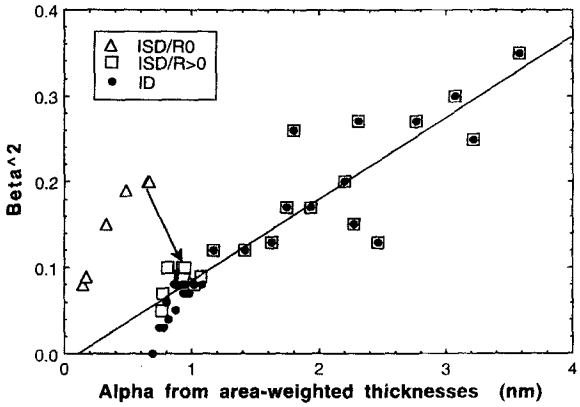


Figure 2. Plot of lognormal parameters $\alpha$ *vs.* $\beta^2$ calculated from the area-weighted thickness distributions of all studied samples (see Table 1). Dark circles: distributions of fundamental particles of illite (ID); open triangles and squares: distributions of fundamental particles of illite + smectite (ISD) of random (R = 0) and ordered (R > 0) clays, respectively. The arrow indicates the trend of the ISD in transition between R = 0 and R = 1. Regression line (see text) refers to the ID.

of particles to count. At $\overline{N}$ = 10, 100 measurements produce a lognormal curve with considerable scatter, but 50 measurements may distort the result considerably by over- or under-estimating both $\alpha$ and $\beta^2$.

*AW ID versus ISD thickness distributions of particles.* The mean of the natural logarithms of the thicknesses (in nm), $\alpha$, is plotted (Figure 2) *versus* the variance of the natural logarithms of the thicknesses (in nm), $\beta^2$, for area-weighted (AW) distributions. These distributions include smectite particles (ISD) and exclude smectite particles (ID). For $\alpha > 1.2$, the plotted curves coincide, because these samples do not contain smectite particles (Table 1). The scatter of data at $\alpha > 1.8$ is related to poor counting statistics (Table 1). At $\alpha < 1.0$, the two sets of data contrast. ID data form a well-defined trend, starting at $\alpha = 0.69$ and $\beta^2 = 0$, where this point correspond to samples consisting only of 2-nm thick particles. ISD data plot close to the ID trend where there are few smectite particles (R = 1 clays). Randomly interstratified (R = 0) clays form a separate trend, starting at $\alpha = 0$ and $\beta^2 = 0$, a point that represents pure smectite (single 2:1 layers), with $\beta^2$ increasing sharply with increasing $\alpha$. In the transition from R = 0 to R = 1 (at $\alpha$ of 0.7), $\beta^2$ of ISD decreases abruptly (note arrow, Figure 2).

*Characteristics of AW-thickness distributions of illite particles.* The ID data, in contrast to ISD, are characterized by a linear trend of $\alpha$ *vs.* $\beta^2$ parameters (Figure 2). No apparent additional trends are detected where samples from different locations are plotted separately.

Figure 3 presents relations for mean area-weighted thicknesses, $\overline{N_a}$, and $\alpha$ and $\beta^2$. If ideal lognormal distributions are assumed, $\beta^2$ also may be calculated using Equation (7) and the regression equation of Figure 3A. The relation obtained in this way, $\beta^2 = -0.02 + 0.09 \ln \overline{N_a}$, is nearly identical to that derived by experiment (Figure 3B), indicating that the experimental data follow the lognormal distribution closely. The precision of the regression equations presented in Figure 3 was considered by fitting only data for $\overline{N_a} < 6$, which have superior counting statistics, and differences in the results were negligible. Combining equations from Figure 3A and 3B produces a linear relationship between $\alpha$ and $\beta^2$ that characterizes ID (Figure 2):

$$\beta^2 = 0.107\alpha - 0.03. \quad (11)$$

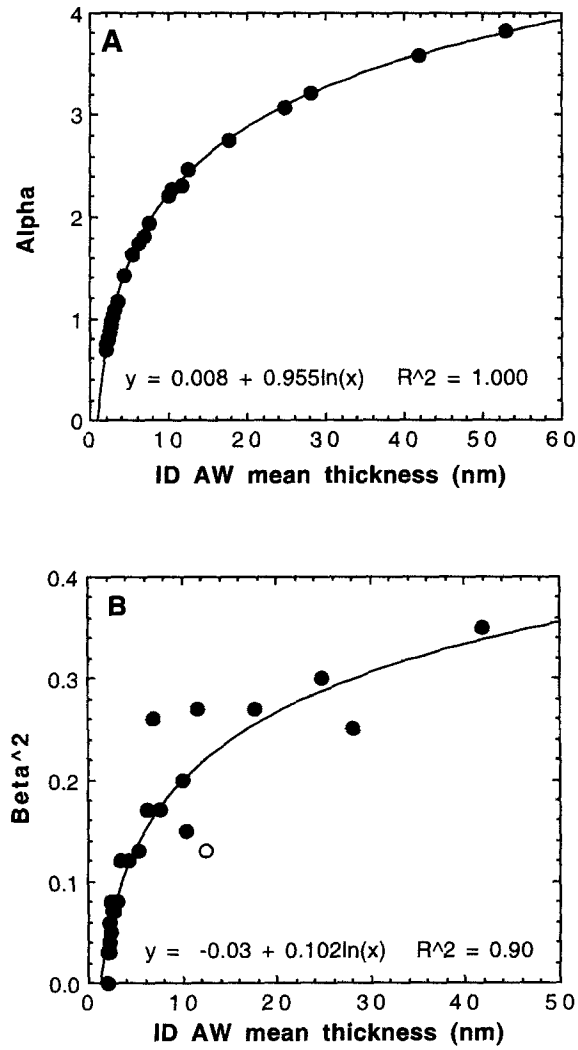


Figure 3. Correlation between mean thickness ($\overline{N_a}$) and lognormal parameters $\alpha$ (3A) and $\beta^2$ (3B) for area-weighted thickness distributions of illite fundamental particles (ID AW). The sample marked with an open circle was not used in the regression analysis, where $R^2$ = the regression coefficient.

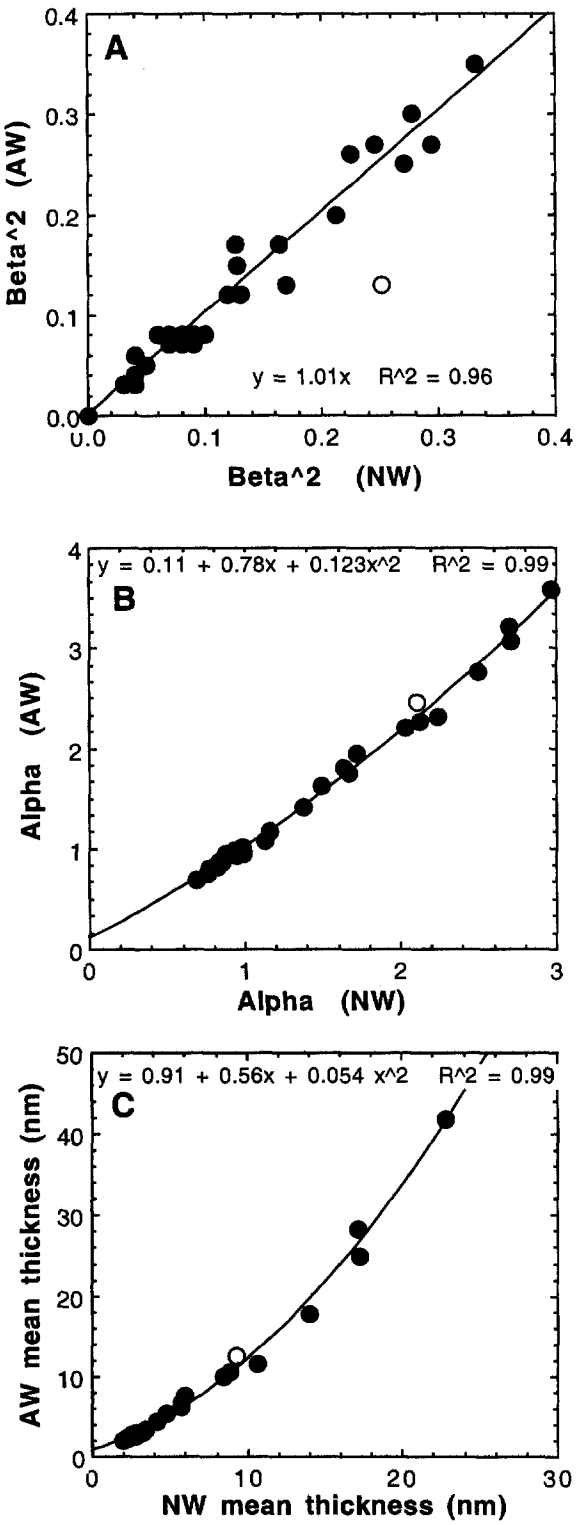


Figure 4. Comparison between area (AW) and number-weighted (NW) thickness distributions for illite particles (ID). The sample marked with an open circle was not used in the regression analysis. (A) comparison between $\beta^2$ values; (B) comparison between $\alpha$ values; (C) comparison between mean thicknesses. $R^2$ is the regression coefficient.

*Area (AW) versus number-weighted (NW) thickness distributions.* Number-weighted ID curves also are lognormal, and are described by similar equations to those in Figure 3. Figure 4 gives regression curves for NW *versus* AW lognormal parameters. Both distributions are related uniquely: with values of $\beta^2$ identical (Figure 4A), but $\overline{N}$ and $\alpha$ values increasing more rapidly for AW than for NW in $\overline{N} > 3$ samples (Figure 4B and 4C). This rapid increase in $\overline{N}$ and $\alpha$ values implies that for $\overline{N_a} > 3$, the thickness and the area of illite particles are positively correlated. Thus, for an identical value of $\beta^2$, $\overline{N}$ and $\alpha$ values are larger for AW than for NW distributions. Figure 4 can be used to calculate AW parameters from NW parameters for these types of clays.

*Evolution of the frequencies of particles of a given thickness during illitization.* Figure 5 shows the evolution of particle thickness during illitization (ISD AW data) in a plot of frequency of particles of a given thickness *vs.* sample mean thickness (an increase in mean thickness is indicative of the progress of the illitization of smectite). Particles appear and disappear in a regular fashion during illitization: thin particles have a greater maximum frequency and occur with a narrower range of $\overline{N}$ than thick particles.

*Fundamental-particle thickness versus mixed-layer crystal thickness.* Mean fundamental-particle thickness ($\overline{N_a}$), mean mixed-layer crystal thickness (T), and "expandability" (*i.e.*, percentage of smectitic interlayers, or %S) are related and characterize mixed-layer clay crystals in the [001]* direction (Drits *et al.*, 1997):

$$\overline{N_a} = 100T/[(T - 1)\%S + 100], \qquad (12)$$

$\overline{N_a}$ and T are means of AW ISD and are given as numbers of layers (equal to the thickness in nm for dehydrated illite-smectite).

Equation (12) may be used to calculate $\overline{N_a}$ from %S and T, the latter measured from XRD peak broadening of K-saturated and dehydrated mixed-layer clays (Drits *et al.*, 1998). $\overline{N_a}$ of ISD distributions may be calculated also from the fixed cations content [Equations (2) and (3) of Środoń *et al.*, 1992]. The XRD method of Bertaut-Warren-Averbach (Drits *et al.*, 1998), when applied to fundamental particles (PVP technique of Eberl *et al.*, 1998b), gives $\overline{N_a}$ for only the population of illite particles (ID), because isolated 2:1 layers do not contribute to diffraction peaks. Thus, if TEM measurements are not available, the PVP technique is the best alternative for determining the thickness distribution for illite fundamental particles.

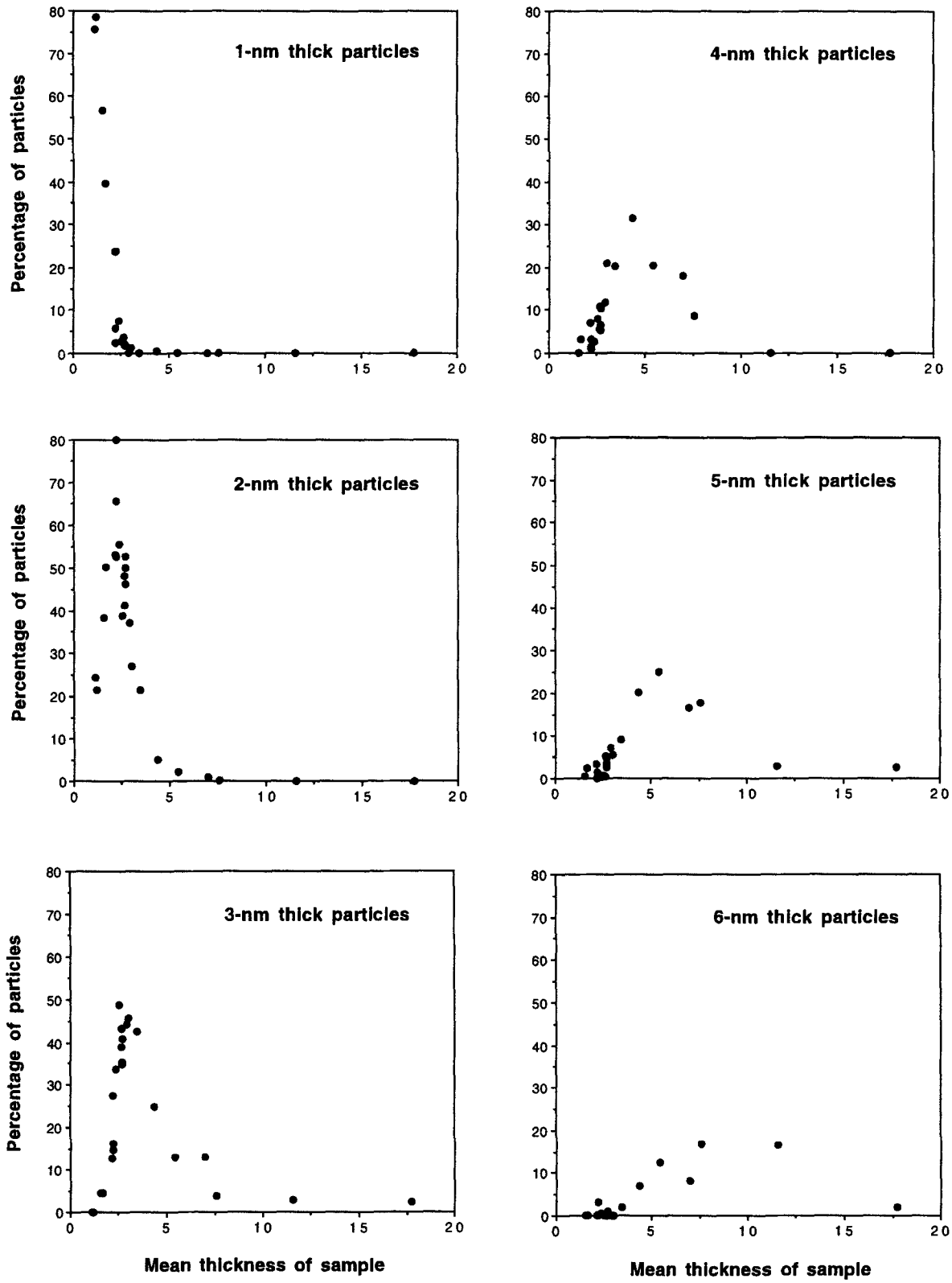
1-nm thick particles
2-nm thick particles
3-nm thick particles
4-nm thick particles
5-nm thick particles
6-nm thick particles
Percentage of particles
Mean thickness of sample
0
5
10
15
20
10
20
30
40
50
60
70
80

*Particle dimensions in the (001) plane*

A positive correlation between the mean thickness and the mean area of illite particles for samples with $\overline{N} > 3$ is shown in Figure 6A. The large scatter of the data can be understood if mean length and mean width are plotted separately against mean thickness (Figure 6B). The two lines in Figure 6B are drawn through minimum values of mean length and mean width for a given mean thickness. These lines correspond to the line drawn through the minimum-area values in Figure 6A. Samples that plot on these lines contain plate-like particles with an aspect ratio (mean length/mean width) of about 2:1. However, many samples plot above these lines, which indicates that these samples have larger mean areas for a given $\overline{N}$ value. These particles are both plate-shaped and lath-shaped, with aspect ratios to 9:1. For $\overline{N} < 10$, Figure 6C indicates that both shapes are found, and at larger $\overline{N}$ values only platy particles occur.

The increase in length and width of particles with increasing thickness is observed also within individual samples, but only for samples with larger particle sizes. These data show scatter (Figure 7A) as do the length *versus* width plots (Figure 7B) and therefore, regression analyses were not obtained. Figure 7B also indicates that smectite and illite particles of a given sample have similar dimensions within the (001) plane and similar aspect ratios.

Most distributions of length and width for individual samples are lognormal. If the lognormal parameters for all samples are plotted together, an approximate increase in $\beta^2$ with $\alpha$ is observed (Figure 8). The trends are sub-parallel, but the data are too scattered to determine reliable regression equations between $\alpha$ and $\beta^2$ for width and length.

## THEORETICAL APPROACH

Most of the samples, collected from seven locations, have lognormal populations of illite fundamental-particle thicknesses. The lognormal parameters $\alpha$ and $\beta^2$ can be calculated from $\overline{N}_a$ (Figure 3) and, for most of the ID samples, $\beta^2$ increases linearly with $\alpha$ [Figure 2 and Equation (11)]. These relations hold despite the fact that the correlations among thickness and dimensions within the (001) plane are not strong (Figure 6). In other words, samples of a given mean particle thickness may be composed of particles with highly variable mean areas and mean elongations, but particle thicknesses follow Equation (11), *i.e.*, a unique path in $\alpha$ *vs.* $\beta^2$ plot. Therefore, it is feasible that each location shows the same growth mechanism along the [001]* direction, and it is this mechanism that is responsible for the generation and the evolution of lognormal distributions.

The mathematical law that generates lognormal distributions is known as the Law of Proportionate Effect (LPE), discovered by Kapteyn (1903). Numerous physical mechanisms operate according to this law and lognormal distributions are therefore common in natural systems. We assume for illite-smectite, that the growth mechanism for fundamental particles along the [001]* direction follows this law. Applied to crystal growth, LPE states that for a given growth cycle, particles will grow in proportion to their size times a random number:

$$X_{j+1} = X_j + \epsilon_j X_j, \quad (13)$$

where $X_j$ and $X_{j+1}$ are crystal dimensions before and after a growth cycle, respectively, and $\epsilon_j$ is a random number between 0 and 1. Lognormal distributions are generated and evolved by repeating growth cycles for a large number of particles.

A computer model (GALOPER) simulates this growth mechanism and other types of crystal growth (Eberl *et al.*, 1998a). A comparison between simulated and measured shapes for crystal-size distributions (CSDs) may yield the crystal-growth mechanism. Surface-controlled, open-system growth involves Equation (13) only, which yields lognormally shaped distributions for which $\beta^2$ increases linearly with $\alpha$. During such growth, the growth rate is limited by how fast crystals can grow given an infinite reservoir of reactants. This "ability to grow" is represented by the $\epsilon_j X_j$ term. During supply-controlled growth, however, the limiting step is the rate at which reactants reach the crystal surface. This growth is modeled by normalizing the amount of growth allowed by Equation (13) to the amount of designated mass available during each growth cycle. During this type of growth, the shape of the CSD based on the previous cycle is preserved as the mean size increases (*i.e.*, $\beta^2$ is constant with increasing $\alpha$). Simultaneous nucleation and growth is modeled by permitting nuclei of a specified size to form at a constant or variable nucleation rate, while earlier-formed nuclei grow according to the LPE. This mechanism yields an "asymptotically" shaped CSD, and $\beta^2$ increases exponentially with $\alpha$. The GALOPER program also models Ostwald ripening (*i.e.*, simultaneous dissolution of small particles and growth of larger ones) using equations for supply- and surface-controlled ripening. During this process, $\beta^2$ generally decreases as $\alpha$ increases, and the shape

←

Figure 5. Percentage of particles of a given thickness in a sample (%) *vs.* sample mean thicknesses ($\overline{N}_a$) which is a measure of the progress of the reaction. Both data are for area-weighted distributions of illite + smectite (ISD) fundamental particles. Plots illustrate how particles of a given thickness appear and disappear in the course of illitization.

of the CSD approaches a steady-state, reduced, negatively skewed profile. A detailed discussion of all these models is presented by Eberl *et al.* (1998a).

## INTERPRETATION OF THE ID AND ISD DATA

### *Interpretation of the ID curves*

The experimental ID data (solid circles in Figures 2 and 9) and the data for mean length and mean width (Figure 8), which shows more scatter, support a predominantly surface-controlled growth mechanism for fundamental illite particles, because $\alpha$ and $\beta^2$ are positively correlated. The ID data in Figure 2 are simulated using GALOPER (Figure 9A) by assuming a brief period, during which 2-nm thick illite crystals nucleate and grow (line 1 in Figure 9A for which $\alpha$ and $\beta^2$ are exponentially related), followed by surface-controlled growth without simultaneous nucleation (line 2 for which $\alpha$ and $\beta^2$ are linearly related).

In the GALOPER program, 2-nm thick crystals are permitted to nucleate in two steps. In the first step, 500 2-nm thick crystals nucleate, followed by a the second step where 500 more crystals nucleate while the first 500 crystals grow one step according to the LPE [Equation (13)]. During this process, the relation between $\alpha$ and $\beta^2$ follows curve 1 in Figure 9A. Thereafter, the 1000 crystals continue to grow according to Equation (13) (*i.e.*, surface-controlled growth) without additional nucleation, and the parameters are now related by curve 2 in Figure 9A. The simulation of the ID data can not distinguish whether the initially formed 2-nm thick illite crystals nucleate on previously formed smectite crystals, if they are formed by the coalescence of two smectite layers adjacent to an interlayer potassium, or if they are completely neoformed. Each of these mechanisms produces identical relationships between $\alpha$ and $\beta^2$ for the ID curves during nucleation step. After nucleation, however, surface-controlled growth [Equation (13)] is the only process we have found that can duplicate the experimental relationship described by curve 2.

As noted above, Ostwald ripening decreases $\beta^2$ with increasing $\alpha$, and during supply-controlled growth $\beta^2$ remains constant with increasing $\alpha$. GALOPER calculations indicate that crystal coalescence as the sole process where existing particles are bound by interlayer potassium to form thicker particles is not consistent with the experimental $\alpha$ *vs.* $\beta^2$ plot. In addition, these mechanisms do not yield lognormal CSDs.

Complementary evidence for the proposed mechanism is obtained by comparing the shapes of ID curves at two postulated stages of the reaction: nucleation and growth (at R = 0) *versus* pure growth (R > 0 clays). As noted above, the nucleation and growth mechanism produces "asymptotic" distributions, and pure growth produces lognormal distributions. Figure 10 presents two pairs of ID (R = 0 and R > 0) selected for close

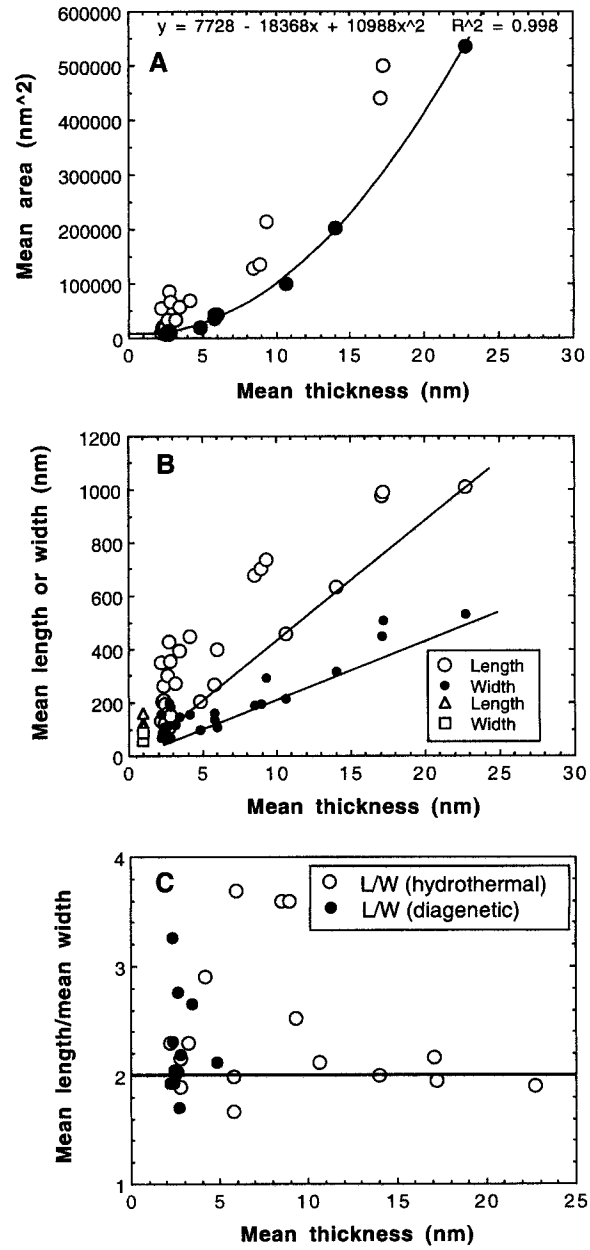


Figure 6. Relations for fundamental particles among: (A) mean thickness ($\overline{N}$) and mean area in the (001) plane; (B) mean thickness and mean length or mean width; and (C) mean thickness and ratio of mean length to mean width for all studied samples. Line in (A) is drawn through the minimum area values. Lines in (B) and (C) represent 2:1 ratio of mean length/mean width. Squares and triangles in (B) represent plots of mean dimensions of smectite particles in randomly interstratified clays.

means. The difference in curve shapes is striking. The samples with R > 0 have shapes that are lognormal, as is shown by the models. In contrast, the curve shapes for samples with R = 0 deviate from lognor-

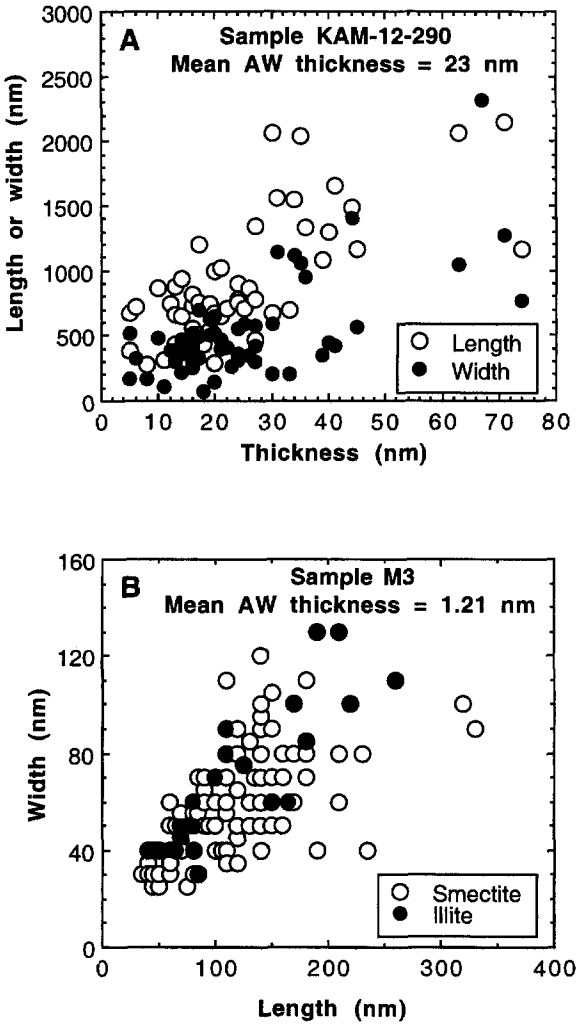


Figure 7. Relations among length, width, and thickness of individual fundamental particles in two samples, one with a large $\overline{N_a}$ (A), and the other with a small $\overline{N_a}$ (B).

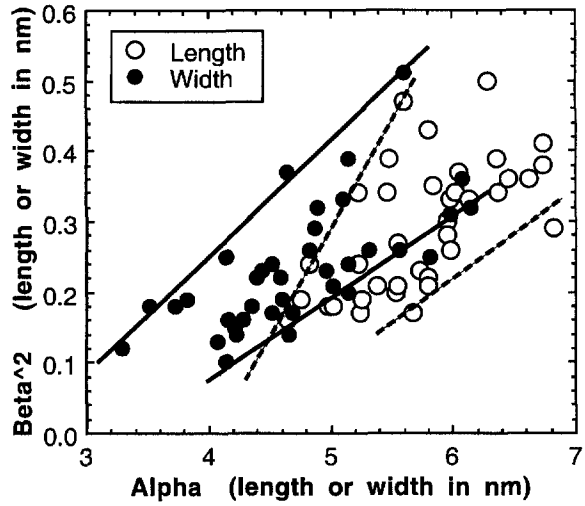


Figure 8. Plot of lognormal parameters calculated for length and width distributions of fundamental particles. Data are scattered, but approximate parallel trends occur for lines drawn contouring the plot areas for width (solid lines) and length (dashed lines).

mality. These samples are dominated by the finest particles, which is characteristic of simultaneous nucleation and growth.

This specific shape (asymptotic) of curves for ID of R = 0 clays is inconsistent with an alternative hypothesis, *i.e.,* illite growth from a smectite nucleus. If illitization proceeds by nucleation of smectite, followed by growth of the single layer nuclei into illite particles, the resulting ID curves would be strictly lognormal, as confirmed by modeling.

*Interpretation of the ISD curves*

A successful model of the illitization mechanism must explain also the evolution of the ISD illustrated in Figure 2. Figure 9B presents a GALOPER simulation that is consistent with the experimental data. The simulation involves decaying nucleation and growth, followed by pure growth. From experimental evidence (Table 1), the pure nucleation stage probably ends when the clay contains ~75% single layers and 25% double layers, and the nucleation and growth follows. The process consumes single layers which become exhausted at near the mean thickness of 2.5 nm, in agreement with the experimental data. Pure surface-controlled growth follows.

The consumption of single layers during illitization is illustrated in Figure 11, where the percentages of single layers in the ISD *versus* mean thickness of ISD or ID is plotted. The means are measures of the progress of the reaction. Three models of growth are evaluated, each starting from the same pure nucleation stage, which is 75% single layers and 25% double layers. The simulations show that pure growth is incapable of consuming the available single layers at the rate indicated by experimental data. The mechanism for the fast consumption of single layers is nucleation. This mechanism consumes all the available single layers, and no additional dissolution and reactant removal mechanism is required. The best fit of the experimental data is obtained when the model of decaying nucleation accompanied by growth is applied (Figure 11).

## CONCLUSIONS

Analysis of the illite fundamental-particle thickness distributions measured by TEM indicates the operation of a unique growth mechanism. Figure 12 shows the relationship between the expandability along [001]* direction as measured by XRD (%S) and the percentage of single layers in the ISD as measured by TEM. These two measurements are not compatible: %S > 0

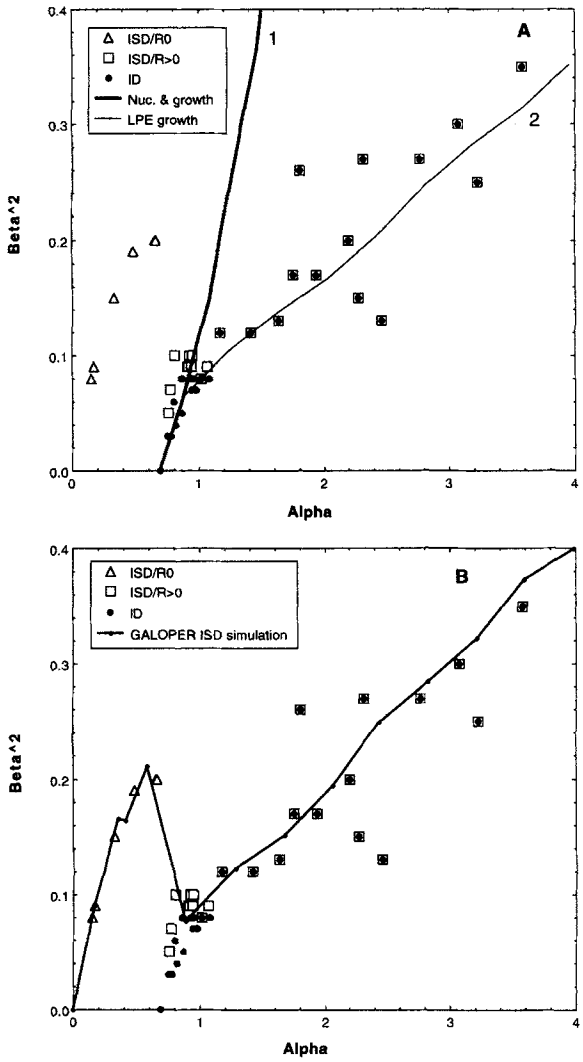


Figure 9. Data from Figure 2 and Table 1 plotted with lines representing different growth mechanisms modeled using GALOPER (see text). (A) Simulations for the ID. Line 1 is for the mechanism of nucleation and growth, and line 2 is for surface-controlled (LPE) growth. (B) Simulation of the ISD from the reaction pattern discussed in the text. See Figure 2 for symbols.

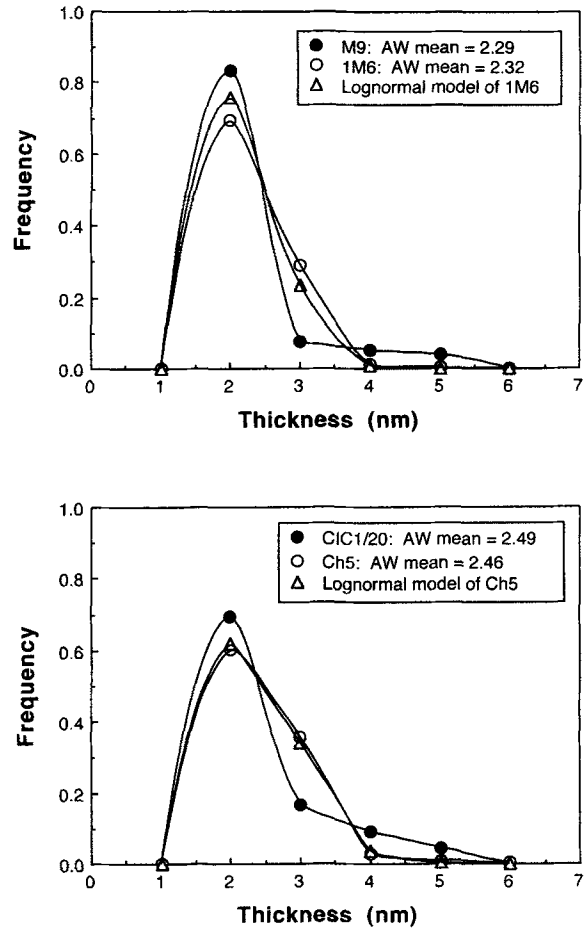


Figure 10. Pairs of experimental values of ID of R = 0 (filled circles) *vs.* R > 0 (empty circles) illite-smectite samples selected to have similar mean values. R > 0 clays are strictly lognormal, as shown by the model (triangles), whereas R = 0 clays strongly deviate from lognormality owing to excess of 2-nm particles.

even when single layers are absent owing to the interparticle diffraction between illite fundamental particles (Nadeau *et al.*, 1984). Three stages of the process as discussed above are shown in the plot: 1) The nucleation of 2-nm thick crystals at the incipient stage of illitization, until a clay containing 75% single layers forms (at ~70%S as measured by XRD); 2) The simultaneous nucleation and growth of 2-nm nuclei in the 75–0% single layer range (70–20%S). Simulations of this stage imply a process where illite crystals nucleate and grow at the expense of single layers, possibly in a closed system. The nucleation occurs at a decaying rate, thus for R = 0 clays (>10% single layers) nucleation dominates the process, and for R > 0 clays (<10% single layers) growth is dominant; 3) Surface-controlled growth (single layers absent, <20%S) proceeds in three dimensions, unlike stage 2. Because all single layers have been consumed, the origin of the reactants to grow illite in this stage is uncertain. Illite growth may be supported by the dissolution of amorphous material or other minerals (*e.g.*, feldspar) in the bentonites or in the adjacent wall rock, by percolating reactant-rich solutions, or by random dissolution (random with respect to illite-particle thickness) of previously formed illite crystals. The latter mechanism, called surface-controlled random ripening (Eberl *et al.*, 1998a) is effective only if the supply of reactants from dissolution of unstable illite particles is faster than the reactant use by the growth of

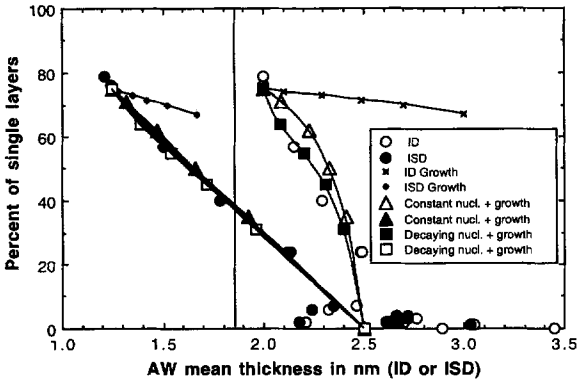


Figure 11. Plot of percent of single layers in ISD *vs.* means ($\overline{N_a}$) of ID and ISD to illustrate the rapid depletion of single layers during illitization. The experimental data are fitted with lines representing modeling by GALOPER of surface-controlled growth of 2-nm nuclei in three versions: pure growth, growth plus constant rate nucleation, and growth plus decaying rate nucleation. The latter model produces the best fit.

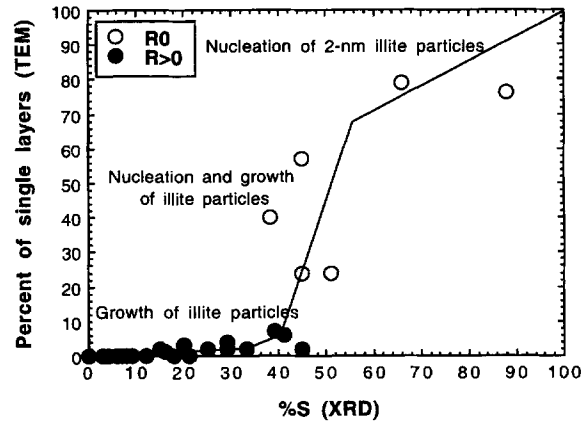


Figure 12. Plot of % smectite measured by XRD (%S) *vs.* percent of single layers in ISD measured by TEM, which reflects three stages of the smectite illitization process: nucleation, nucleation and growth, and surface-controlled growth. empty circles = random clays, filled circles = ordered clays.

stable illite particles. The analysis excludes Ostwald ripening as an illite growth mechanism.

The appearance of illite fundamental particles in between smectite single layers produces R = 0 mixed layering. Dissolution of smectite (single layers), nucleation of illite (double layers), and growth of illite fundamental particles all result in the evolution of the mixed-layer crystals towards more illitic composition and explain the transition from R = 0 to R = 1. Note that this transition occurs during the second stage of the illitization process. Clays identified by XRD as R = 1 or R = 2 still contain some single layers (Table 1), which are consumed slowly during stage 2 of the process. Rapid depletion of single layers in R = 0 clays is caused by nucleaction (Figure 11). Of course, if nucleation is not sufficiently intense, an alternative mechanism may be the removal of the excess reactants produced by the dissolution of single layers in an open system.

The data in this paper are limited to illite formed from smectite in altered pyroclastic rocks and bentonites but the proposed model may explain also the shape of %S *vs.* depth (or temperature) plots for illite-smectite from shales of sedimentary basins. These plots show a marked decrease of %S per unit depth or temperature at early stages of the reaction, and small or unmeasureable decreases below 15%S (*e.g.*, Jennings and Thompson, 1986; Šucha *et al.*, 1993). If the reaction involves growth of illite crystallites in a smectite matrix, the growth by one layer from a mean of 2 nm to a mean of 3 nm corresponds to a decrease from nearly 100%S (R = 0 clays) to 15%S (R > 1 clays). Further decrease to 5%S corresponds to an increase in mean crystallite thickness from 3 to 10 nm (Table 1). Therefore, illitization may only appear to cease at 15%S because %S is a non-linear indicator of the progress of reaction.

Figure 5 suggests why only R = 1 clays often form regular interstratifications. Regular interstratification implies a perfect alternating pattern, such as ABABAB or ABBABBABB. Such patterns correspond to a sample containing fundamental particles of a unique thickness. The mechanism of illitization allows for such particle-thickness distribution only at the beginning of the process, where a sample may be composed primarily of 2-nm thick particles. The optimal conditions for the occurrence of regularly interstratified R = 1 clay are an intense nucleation of 2-nm particles leading to complete dissolution of single layers before substantial numbers of 3-nm and thicker particles could be grown. Later in the growth process, distributions spread out (Figures 1 and 5) and a regular interstratification cannot be realized.

Our data relating the area of the (001)* plane and particle length *vs.* width dimensions with increasing particle thickness indicate that, at least until $\overline{N}$ = 3, growth seems to proceed only in the [001]* direction: no correlation between particle thickness and area is observed (Figures 4C and 6A). The large variation of particle area and shape among different samples at this stage of illitization seems to be related to original variations in the dimensions of nuclei. This conclusion is supported by the same size and shape of smectite and illite particles in a given sample (Figure 7B). For coarse samples, elongated shapes do not occur (Figure 6C), and a positive correlation between mean thickness and area (Figure 6A) indicates three-dimensional growth.

The absence of major morphological changes at early stages of illitization has been presented as the best evidence that smectite alters to illite by a solid-state

transformation (SST mechanism; Altaner and Ylagan, 1997; Cuadros and Altaner, 1998). However, an alternative hypothesis is that illite nuclei precipitate between smectite layers, and that lateral growth along the (001) plane is dependent on the dimensions of the smectite layers. Three-dimensional growth begins when all of the smectite layers are dissolved.

## ACKNOWLEDGMENTS

This research was made possible by the financial support of the U.S. Geological Survey to V. Drits and J. Środoń. Special thanks to R. Krushensky and P. Hearn of the Office of International Geology. V. Šucha and A. Inoue kindly supplied TEM measurements of their samples. We thank S. Altaner, A. Blum, H. May, D. McCarty, and R. Pollastro for reviewing the original manuscript.

## REFERENCES

Altaner, S.P. and Ylagan, R.F. (1997) Comparison of structural models of mixed-layer illite/smectite and reaction mechanisms of smectite illitization. *Clays and Clay Minerals,* **45,** 517–533.

Altaner, S.P., Weiss C.A., and Kirkpatrick R.J. (1988) Evidence from $^{29}$Si NMR for the structure of mixed-layer illite/smectite clay minerals. *Nature,* **331,** 699–702.

Benjamin, J.R. and Cornell C.A. (1970) *Probability and Decision for Civil Engineers.* McGraw Hill Book Co., New York, 684 pp.

Clauer, N., Środoń, J., Francu, J., and Šucha, V. (1997) K-Ar dating of illite fundamental particles separated from illite-smectite. *Clay Minerals,* **32,** 181–196.

Cuadros, J. and Altaner, S.P. (1998) Characterization of mixed-layer illite-smectite from bentonites using microscopic, chemical, and X-ray methods: Constraints on the smectite-to-illite transformation mechanism. *American Mineralogist,* **83,** 762–774.

Drits, V.A., Środoń, J., and Eberl, D.D. (1997) XRD measurement of mean illite crystallite thickness: Reappraisal of the Kubler index and the Scherrer equation. *Clays and Clay Minerals,* **45,** 461–475.

Drits, V.A., Eberl, D.D., and Środoń, J. (1998) XRD measurement of mean thickness, thickness distribution and strain for illite and illite/smectite crystallites by the Bertaut-Warren-Averbach technique. *Clays and Clay Minerals,* **46,** 461–475.

Eberl, D.D. and Środoń, J. (1988) Ostwald ripening and interparticle diffraction effects for illite crystals. *American Mineralogist,* **73,** 1335–1345.

Eberl, D.D., Środoń, J., Lee, M., Nadeau, P.H., and Northrop, H.R. (1987) Sericite from the Silverton caldera, Colorado: Correlation among structure, composition, origin, and particle thickness. *American Mineralogist,* **72,** 914–935.

Eberl, D.D., Środoń, J., Kralik, M., Taylor, B., and Peterman, Z.E. (1990) Ostwald ripening of clays and metamorphic minerals. *Science,* **248,** 474–477.

Eberl, D.D., Drits, V.A., and Środoń, J. (1998a) Deducing growth mechanisms for minerals from the shapes of crystal size distributions. *American Journal of Science,* **298,** 499–533.

Eberl, D.D., Nüesch, R., Šucha, V., and Tsipursky, S. (1998b) Measurement of fundamental illite particle thickness by X-ray diffraction using PVP-10 intercalation. *Clays and Clay Minerals,* **46,** 89–97.

Inoue, A. and Kitagawa, R. (1994) Morphological characteristics of illitic clay minerals from a hydrothermal system. *American Mineralogist,* **79,** 700–711.

Inoue, A., Kohyama, N., Kitagawa, R., and Watanabe, T. (1987) Chemical and morphological evidence for the conversion of smectite to illite. *Clays and Clay Minerals,* **35,** 111–120.

Inoue, A., Velde, B., Meunier, A., and Touchard, G. (1988) Mechanism of illite formation during smectite-to-illite conversion in a hydrothermal system. *American Mineralogist,* **73,** 1325–1334.

Jennings, S. and Thompson, G.R. (1986) Diagenesis of Plio-Pleistocene sediments of the Colorado River delta, southern California. *Journal of Sedimentary Petrology,* **56,** 89–98.

Jiang, W.-T., Peacor, D.R., Arkai, P., Toth, M., and Kim, J.W. (1997) TEM and XRD determination of crystallite size and lattice strain as a function of illite crystallinity in pelitic rocks. *Journal of Metamorphic Geology,* **15,** 267–281.

Kapteyn, J.C. (1903) *Skew Frequency Curves in Biology and Statistics.* Astronomical Laboratory, Noordhoff, Groningen, 69 pp.

Lanson, B. and Champion, D. (1991) The I/S-to-illite reaction in the late stage diagenesis. *American Journal of Science,* **291,** 473–506.

Nadeau, P.H. (1985) The physical dimensions of fundamental clay particles. *Clay Minerals,* **20,** 499–514.

Nadeau, P.H. (1987) Relations between the mean area, volume and thickness for dispersed particles of kaolinites and micaceous clays and their application to surface area and ion exchange properties. *Clay Minerals,* **22,** 351–356.

Nadeau, P.H., Wilson, M.J., McHardy, W.J., and Tait, J.M. (1984) Interstratified clays as fundamental particles. *Science,* **225,** 923–935.

Reynolds, R.C., Jr. (1992) X-ray diffraction studies of illite/smectite from rocks, $<1$ $\mu$m randomly oriented powders, and $<1$ $\mu$m oriented powder aggregates: The absence of laboratory induced artifacts. *Clays and Clay Minerals,* **40,** 387–396.

Reynolds, R.C., Jr. (1985) NEWMOD, a Computer Program for the Calculation of Basal X-Ray Diffraction Intensities of Mixed-Layered Clays. R.C. Reynolds, Hanover, NH. 03755.

Środoń, J., Morgan, D.J., Eslinger, E.V., Eberl, D.D., and Karlinger, M.R. (1986) Chemistry of illite/smectite and end-member illite. *Clays and Clay Minerals,* **34,** 368–378.

Środoń, J., Andreoli, C., Elsass, F., and Robert, M. (1990) Direct high-resolution transmission electron microscopic measurement of expandability of mixed-layer illite/smectite in bentonite rock. *Clays and Clay Minerals,* **38,** 373–379.

Środoń, J., Elsass, F., McHardy, W.J., and Morgan, D.J. (1992) Chemistry of illite-smectite inferred from TEM measurements of fundamental particles. *Clay Minerals,* **27,** 137–158.

Šucha, V., Kraus, I., Gerthofferova, H., Petes, J., and Serekova, M. (1993) Smectite to illite conversion in bentonites and shales of the East Slovak Basin. *Clay Minerals,* **28,** 243–253.

Šucha, V., Środoń, J., Elsass, F., and McHardy, W.J. (1996) Particle shape versus coherent scattering domain of illite/smectite: Evidence from HRTEM of Dolna Ves clays. *Clays and Clay Minerals,* **44,** 665–671.

Viczián, I. (1997) Hungarian investigations of the "Zempleni" illite. *Clays and Clay Minerals,* **45,** 114–115.

E-mail of corresponding author: ndsrodon@cyf-kr.edu.pl

*(Received 6 March 1998; accepted 12 April 2000; Ms. 98-034)*